Doppler Radar Measurements of Turbulence in Marine Stratiform Cloud during ASTEX

A. S. FRISCH

Environmental Technology Laboratory, Boulder, Colorado

D. H. LENSCHOW

National Center for Atmospheric Research, Boulder, Colorado*

C. W. FAIRALL

Environmental Technology Laboratory, Boulder, Colorado

W. H. SCHUBERT

Colorado State University, Fort Collins, Colorado

J. S. GIBSON

Environmental Technology Laboratory, Boulder, Colorado

(Manuscript received 3 June 1994, in final form 26 October 1994)

ABSTRACT

A cloud-sensing Doppler radar is used with a vertically pointing antenna to measure the vertical air motion in clouds during the Atlantic Stratocumulus Transition Experiment. The droplet fall velocity contamination was made negligible by using only measurements during the time the reflectivity was below −17 dBZ. During one day of measurements, the daytime character of the vertical velocity variance is different than that of the nighttime case. In the upper part of the cloud, the variance had a distinct maximum for both day and night; however, the nighttime maximum was about twice as large as the daytime case. Lower down in the cloud, there was a second maximum, with the daytime variance larger than the nighttime case. The skewness of the vertical velocity was negative near cloud top in both the day and night cases, changing to positive skewness in the lower part of the cloud. This behavior near cloud top indicates that the upper part of the cloud is behaving like an upside-down convective boundary layer, with the downdrafts smaller in area and more intense than the updrafts. In the lower part of the cloud, the behavior of the motion is more like a conventional convective boundary layer, with the updrafts smaller and more intense than the downdrafts. The upside-down convective forcing in the upper part of the cloud is due to radiative cooling, with the daytime forcing less because of shortwave warming.

1. Introduction

Marine stratiform clouds play an important role in climate prediction because of their effect on the earth's radiation budget. Their structure and evolution depend to a large extent on the turbulent motions within the clouds that entrain relatively warm, dry air and distribute the resulting mixture throughout the cloud. In the absence of large surface energy fluxes, the major source of buoyant energy for generating this turbulence is longwave radiative cooling at cloud top. Although considerable effort has been devoted to studying turbulence in stratiform cloud, both with observations (e.g., Brost et al. 1982; Slingo et al. 1982a,b; Nicholls 1984; Hignett 1991; Wang and Albrecht 1994) and numerical models (e.g., Deardorff 1980; Moeng et al. 1992), important questions still remain. For example, in situ observations can give some indication of turbulence intensity and eddy structure at several levels above the surface, but it is difficult to obtain concurrent measurements at many levels throughout the cloud layer and to reference the measurements to the cloud boundaries. Therefore, it is difficult to determine the vertical coherence of the eddies generated by radiative cooling at cloud top that extend into the cloud layer. Large eddy numerical simulations (LES) can generate a detailed

* The National Center of Atmospheric Research is sponsored by the National Science Foundation.

Corresponding author address: Dr. Shelby A. Frisch, NOAA/ETL, R/E/ET6, 325 Broadway, Boulder, CO 80303.

three-dimensional field of motion throughout the entire boundary layer but they parameterize the smallest scales and, therefore, are unable to calculate exactly the mixing within grid cells, which with current technology are about 12.5 m on a side (Moeng et al. 1992). Thus, the processes by which air from above the boundary layer becomes commingled with cloudy air are not explicitly calculated. For this reason, measurements of the flow field at several concurrent locations within a stratiform cloud layer can provide a useful dataset to compare with LES, to gain a better understanding of the in-cloud turbulent entrainment and mixing—especially near cloud top.

One way of measuring these motions is with a cloud-sensing Doppler radar. These radars typically operate at K-band frequencies or higher. A Doppler radar operating at these frequencies can use very small droplets, which have negligible fall velocity, as air motion tracers. For example, we estimate that the National Oceanic and Atmospheric Administration/Environmental Technology Laboratory's K_α-band Doppler radar can detect 640 10-μm radius droplets per liter at a 1-km range. This sensitivity gives us the opportunity to measure turbulent motions in clouds that have such low reflectivity that they are not likely to contain drizzle. The measurements can then be used to give profiles of turbulent motions throughout the clouds. In the examples here, we obtained the data in marine stratus during the Atlantic Stratocumulus Transition Experiment (ASTEX). The radar was located on the island of Porto Santo, in the Madeira Islands, about 800 km W of Casablanca, Morocco. The antenna was located on a 90-m cliff about 100 m from shore. During the observations discussed here the wind was nearly onshore, so there should be minimal impact of the island on the cloud-layer turbulence structure.

2. Method

When the radar antenna is pointed vertically, the measured Doppler-shifted velocity is a combination of vertical air motion plus the reflectivity weighted droplet terminal fall speed. To measure the vertical velocity statistics, the droplet fall speed must either be accounted for or be negligible. The radar reflectivity is useful to help discriminate between droplets that are so small that their fall velocity is negligible and droplets that are likely to have fall speeds that are large enough to contribute to the error in the turbulence measurement. This is because the fall speed is proportional to the square root of the droplet radius in our range of interest (0–40 μm), while the reflectivity is proportional to the sixth power of the radius. Thus, the existance of only a few droplets with higher fall speeds gives a very large increase in radar reflectivity. Since the reflectivity is also proportional to the number of droplets, large variations in droplet concentration have a relatively small effect on reflectivity compared with changes in droplet radius. Thus, even if there are many small droplets, the radar reflectivity will be small compared with the radar reflectivity of a few large droplets that have a large fall speed.

In devising a procedure to screen out data that may have significant fall velocities, we first assume a cloud droplet distribution with known cloud parameters to estimate the Doppler shift of the cloud droplets. In this way, we can estimate a reflectivity that should give a threshold below which the droplet fall speed is a small fraction of typical turbulent fluctuations in vertical air velocity. We then measure the Doppler shift and reflectivity over a time period long enough to get a wide variation in reflectivities. If the fall speed is not contaminating the air motion measurements, there should be no correlation between the velocity measurement and the reflectivity. However, when the reflectivity becomes large enough, we would expect to see an increase in mean vertical velocity with increasing reflectivity, since the larger, more reflective droplets have a higher fall speed.

3. Model

The cloud droplet model we used is a lognormal distribution with three free parameters. This distribution has been used for rain droplets by, for example, Borovikov (1961), Levin (1961), Atlas et al. (1989), and White et al. (1991) and has been used to characterize cloud droplets by Davidson et al. (1984). A similar procedure was used by Frisch et al. (1995) in estimating drizzle and cloud droplet parameters in cases of ASTEX stratiform cloud with drizzle. If we wish to keep our vertical velocity variance error estimates to 10% or less, and if the variance is 0.1 m^2 s^{-2}, then we wish to limit the mean Doppler shift due to the fall velocity of the cloud droplets to less than 0.1 m s^{-1}.

The droplet concentration spectrum is given by

$$n(x) = \frac{N}{\sigma_x\sqrt{2\pi}} \exp[-(x - x_0)^2/2\sigma_x^2], \qquad (1)$$

where $x = \ln(r)$, $x_0 = \ln(r_0)$, r_0 is the modal radius in microns, N is the total number of drops per unit volume, and σ_x is the logarithmic width of the distribution. The reflectivity factor Z for this distribution of droplets is given by

$$Z = 2^6 N\langle r^6\rangle = 2^6 N r_0^6 \exp(18\sigma_x^2), \qquad (2)$$

where the brackets indicate the expected value, and we have used the fact that

$$\langle r^k\rangle = N^{-1}\int_{-\infty}^{\infty} r^k n(x)dx = N^{-1}\int_0^{\infty} r^k n(r)dr$$
$$= r_0^k \exp(k^2\sigma_x^2/2). \qquad (3)$$

The cloud liquid water concentration is given by

$$q_l = (4\pi/3)\rho_w N\langle r^3\rangle = (4\pi/3)\rho_w N r_0^3 \exp(9\sigma_x^2/2), \quad (4)$$

where σ_w is the density of liquid water. The backscattered radar signal from the droplet distribution is characterized by the total backscattering cross section η. The incremental scattering contribution of each size droplet (Battan 1973) is

$$\frac{\partial\eta}{\partial r} = 4\pi(2\pi/\lambda)^4 K^2 r^6 n(r), \quad (5)$$

where $K^2 = 0.93$ is the refractive index factor for liquid water and λ is the radar wavelength. Thus, η is the integral of (5) over all droplets:

$$\eta = \int_0^\infty \frac{\partial\eta}{\partial r}\, dr = \pi^5 \lambda^{-4} K^2 Z. \quad (6)$$

The reflectivity factor Z is related to the more commonly measured radar reflectivity dBZ by

$$\text{dBZ} = 10\log(Z) + 180, \quad (7)$$

where the factor of 180 results because Z is expressed in units of m^3, while the dBZ notation assumes conventional units of $mm^3\ m^{-3}$.

The Doppler spectrum $\partial\eta/\partial V_f$ is defined as the backscatter intensity between Doppler velocities $V_f - dV_f/2$ and $V_f + dV_f/2$ or the reflectivity-weighted velocity distribution. This spectrum is related to the backscatter distribution defined in (5) through the fall velocity dependence on radius,

$$\frac{\partial\eta}{\partial V_f} = \frac{\partial\eta}{\partial r}\frac{\partial r}{\partial V_f} = 4\pi(2\pi/\lambda)^4 K^2 r^6 \frac{\partial r}{\partial V_f} n(r). \quad (8)$$

The kth moment is expressed as

$$\langle V_f^k\rangle_D = \eta^{-1}\int_0^\infty V_f^k \frac{\partial\eta}{\partial V_f}\, dV_f = \eta^{-1}\int_0^\infty [V_f(r)]^k \frac{\partial\eta}{\partial r}\, dr = \langle r^6[V_f(r)]^k\rangle/\langle r^6\rangle, \quad (9)$$

where $\langle\ \rangle_D$ denotes a velocity moment taken from the Doppler spectrum.

Because we want $\langle V_f\rangle_D$ to be less than 0.1 m s^{-1}, we can use Stokes's law and (9) to determine the modal radius and other cloud parameters to obtain the reflectivity maximum. Stokes's law is

$$V_f = k_1 r^2, \quad (10)$$

where $k_1 = 1.19\cdot 10^6\ cm^{-1}\ s^{-1}$. Then using (3), (9), and (10) we can solve for the modal radius in terms of the Doppler shift:

$$r_0 = \left[\frac{\langle V_D\rangle}{k_1}\exp(-2\sigma_x^2)\right]^{1/2}. \quad (11)$$

Using a value of 0.1 m s^{-1} will give a modal radius of approximately 12 μm.

Stratus studies that have measured the droplet spectrum have shown that N is approximately constant with height (e.g., Slingo et al. 1982a,b; Caughey and Kitchen 1984; Nicholls 1984). Furthermore, the droplet distributions can be fit with a lognormal standard deviation of about 0.35. If we use 0.35 for the lognormal width, 12 μm as the modal radius, and 10 droplets per cm^3 as a concentration, then the calculated reflectivity from (2) is about -17 dBZ. In most cases, of course, the number will be much larger than 10 droplets per cm^3. Thus our estimate is very conservative.

To test this, we have taken radar measurements for cases with and without drizzle and plotted the Doppler velocity versus reflectivity for radar range gates 18 and 29, which are about 880 m and 1330 m above sea level, respectively. Each range gate has a length of 37.5 m. For the drizzle case, we plotted range gate 18. These results are shown in Figs. 1, 2, and 3. In the nondrizzle cloud case, we have used the linear data output channel instead of the logchannel for the reflectivity measurements because it is more sensitive. However, this channel saturates at about -4 dBZ for range gate 18 and at about -2 dBZ at range gate 29. This shows up in Figs. 1 and 2 as a maximum limit in the dBZ data. In both of these figures, the plots show no indication of any dependence of the vertical velocity on reflectivity. There is a slight negative downward motion at the lowest reflectivity that is probably caused by the island. At other times there was a continuous upward velocity persisting for several hours. These low-frequency vertical velocities are removed from the turbulence calculations. The third figure, which is a cloud drizzle

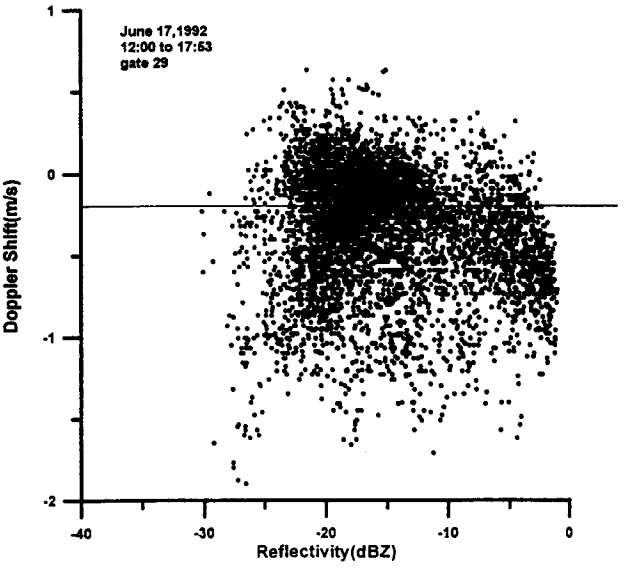

FIG. 1. Vertical velocity vs reflectivity for range gate 29 at 1294-m altitude, near cloud top.

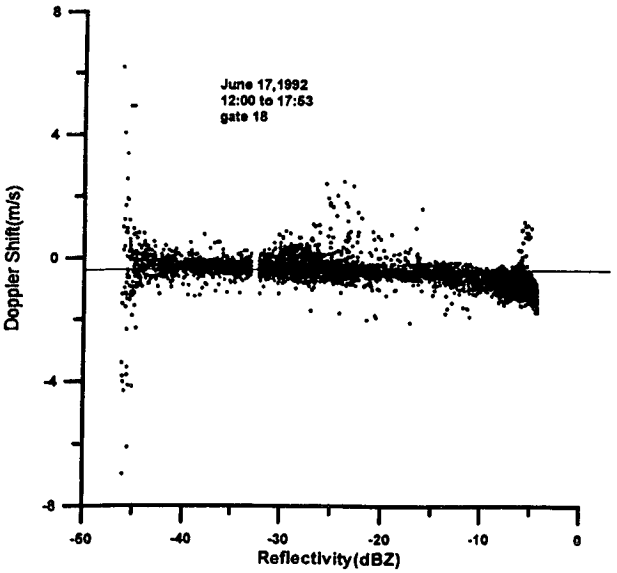

FIG. 2. Vertical velocity vs reflectivity for range gate 18 at 822-m altitude.

case, shows a strong dependence of velocity on reflectivity above our threshold reflectivity of −17 dBZ. This is evidence that data below −17 dBZ should give a good turbulence measurement with negligible contamination by larger droplets.

As an additional constraint, we do not report turbulence quantities from a particular range gate if the total number of available points is less than 20% of the measurement time interval.

4. Cloud turbulence measurements

We present here data taken in the early morning before sunrise and near midday on 17 June 1992. This day was selected because stratus clouds persisted throughout almost the entire time period with relatively little change in height and reflectivity, and there were periods of time when the reflectivity throughout the cloud layer was less than −17 dBZ (thus indicating an absence of significant drizzle). Incorporating both nighttime and daytime periods permits us to investigate the effect of solar radiation on the turbulence structure of stratus. In the nighttime case, we selected time periods starting at 0030, 0230, 0300, 0330, 0400, and 0430 UTC. For the daytime case, we chose the time intervals from 1200 to 1530 UTC. These particular time periods were selected because there was measurable velocity and radar echo below our threshold during a significant part of the time. This enabled us to get longer datasets to compute the turbulence quantities. The radar operated in a vertical mode for 23 min of every half hour with a measurement at each range gate every 3 s. Each range gate was 37.5 m apart vertically, with the first gate 150 m above the radar. Figure 4a is a sample measurement for range gates 3–34 over two of the 23-min periods. In this particular case, we show data from 0230 to 0323 UTC. To display all gates simultaneously we have offset each successive gate by 2 m s^{-1}. Data above the −17 dBZ threshold are not included; these regions are plotted as zero relative velocity. If the signal strength was too small to measure the vertical velocity, the velocity was also set to 0 plus the appropriate offset. An example of this thresholding is at gates 8, 9, and 10 at the beginning of the displayed time interval. Each of these gates shows a flat region persisting for a minute or longer. The velocity has been set to zero plus the appropriate multiple of 2 m s^{-1}. In most of this figure, the loss of a measurement was due to higher reflectivity rather than loss of signal, except at the top of the cloud where the signal was too small to be measured.

From this figure, it is apparent that in the upper part of the cloud the downdrafts are more intense with less area than the updrafts. The reverse is true in the lower part of the cloud. These updrafts and downdrafts are coherent for several tens of meters. For example, at 2.8 h there is an indication of a slight velocity perturbation at gate 31, which at gate 30 is a much stronger downdraft growing in intensity to a maximum at gate 26 or 27 and then diminishing to almost nothing by gate 22, a distance of 262 m from the top to the bottom of the downdraft.

We can contrast the nighttime vertical wind fluctuations with the daytime case shown in Fig. 4b. This case starts at 1200 UTC, and ends at 1253 UTC. Like the previous case, there is a 7-min gap beginning 23 min after every half hour because of other scans with the radar. This set of observations shows a different

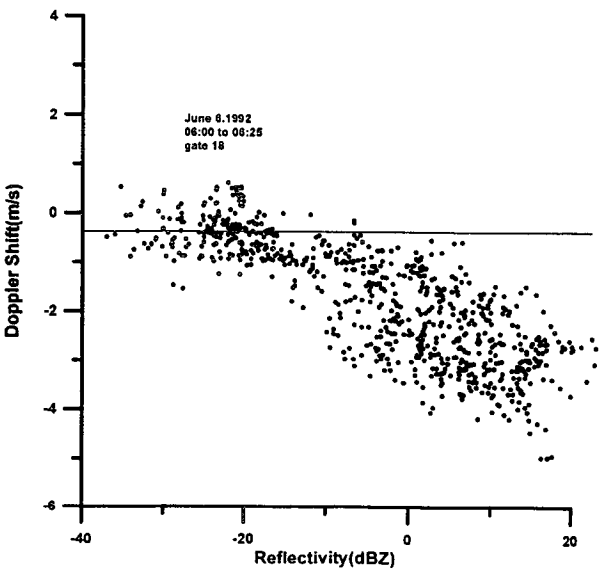

FIG. 3. Vertical velocity vs reflectivity for range gate 18 at 822-m altitude, with drizzle.

character in the vertical velocity field compared with the nighttime case. Here, the downdrafts are much weaker and coherent for shorter distances in the upper part of the cloud, although they are still stronger than the updrafts. However, in the lower part of the cloud, the updrafts are much stronger and coherent for much longer vertical distances. For example, the updraft at the end of the display shows a strengthening with height, starting at gate 4 and growing in intensity until gate 17 and then decreasing in strength until about gate 22, where it is almost undetectable. This is a distance of 675 m. In the daytime case, the blank regions of no data are almost entirely due to low signal strength rather than being thresholded by too high reflectivity.

5. Analysis of variance and skewness

The day and night variances are shown in Fig. 5. The variances were computed by using the vertical velocity measurements only when the reflectivity was less than -17 dBZ. The mean vertical air motion was computed for the entire 23-min time interval and removed from the vertical velocity. Then the variance and skewness were computed from the resulting velocity fluctuations. With a 10 m s^{-1} mean wind speed, this would correspond to an averaging length of 14 km. In both cases, the variance shows two maxima, one in the upper third of the cloud and the other near cloud base. In the nighttime case the upper-level variance is larger than the lower level, while in the daytime case the opposite is true. The presence of two maxima suggests that there are two sources of turbulence energy—one near cloud top and the other near cloud base. The upper maximum is consistent with what we see in Fig. 4, where the velocity fluctuations at the top level are noticeably less than at the underlying level.

The vertical velocity skewness displayed in Fig. 6 shows that the skewness is negative for both daytime and nighttime cases in the upper part of the cloud. This supports the interpretation that the maximum variance in the upper part of the cloud is due to cloud-top radiational cooling. Positive skewness is expected if the main source of turbulent energy is buoyancy introduced from below cloud base or generated from condensation near cloud base. Thus, the positive skewness observed just above cloud base for both cases supports the possibility of positive buoyant flux near cloud base. This may be the result of significant positive surface buoyancy flux or radiational warming (or both). The fact that the variance increases rapidly from a value near the noise level of the velocity measurement at cloud base (about 300 m) to a maximum about 40% of the distance between cloud base and the variance minimum (about 1100 m, where the skewness becomes negative), suggests that the buoyancy flux originates near cloud base rather than at the surface. The larger daytime variance maximum and larger skewness near cloud base suggest a larger buoyancy flux at cloud base in the daytime. It is not obvious why this should be the case, since, if anything, the shortwave warming should act to increase the stability near cloud base. We do not believe this lower maximum is a mixing effect of the island, since any convection generated by the heating of the island would not have time to be felt at cloud base. Our downwind distance from the island's edge was about 100 m, and even with a vertical velocity scale of 1 m s^{-1}, with a 10 m s^{-1} mean wind, the height scale for the island convection at this distance downwind would be 10 m. On the other hand, the larger nighttime maximum near cloud top is consistent with shortwave warming canceling out part of the effect of longwave cooling near cloud top during the daytime.

To make sure that the variances are primarily due to buoyancy generation, we consider the possibility of turbulence generation by shear. A wind profiler operated by Colorado State University next to the radar provided 12 wind profiles per hour. The profiles for the east–west and north–south components are shown in Figs. 7 and 8 for the daytime and nighttime cases that were averaged over the same time intervals as the radar variance and skewness measurements. From these profiles, we calculated the mean shear as a function of height, which is shown in Fig. 9. Cloud top is at about 1.4 km, and below this height the nighttime shear is about a factor of 2 less than the daytime shear. With these differences, and the fact that in the upper part of the cloud the skewness is negative, it seems unlikely that the day–night differences in the vertical velocity variances are due to shear generation. In the lower part of the cloud, the nighttime shear is several times larger than the daytime shear, and the daytime variance maximum is larger than the nighttime case, so the shear is probably not the cause of this larger daytime cloud base maximum.

We can use the radar variance measurements to estimate the magnitude of the virtual temperature and temperature fluxes at cloud top. Nicholls (1988) has shown—using aircraft observations in the upper part of marine stratus driven by radiative cooling—that the maximum of the vertical velocity variance σ_w^2 normalized by a convective velocity scale w_* approximately satisfies

$$(\sigma_w^2)_{\max}/w_*^2 \approx 0.4, \tag{12}$$

where

$$w_*^3 = 2.5\left(\frac{g}{T_v}\right)\int_{z_1}^{z_2} \overline{wT_v}\,dz \tag{13}$$

and T_v is the virtual temperature. The data of Nicholls (1988) show an approximately linear decrease of wT_v with height from the cloud top z_2 down to the base of the turbulent layer z_1. Thus, assuming the form

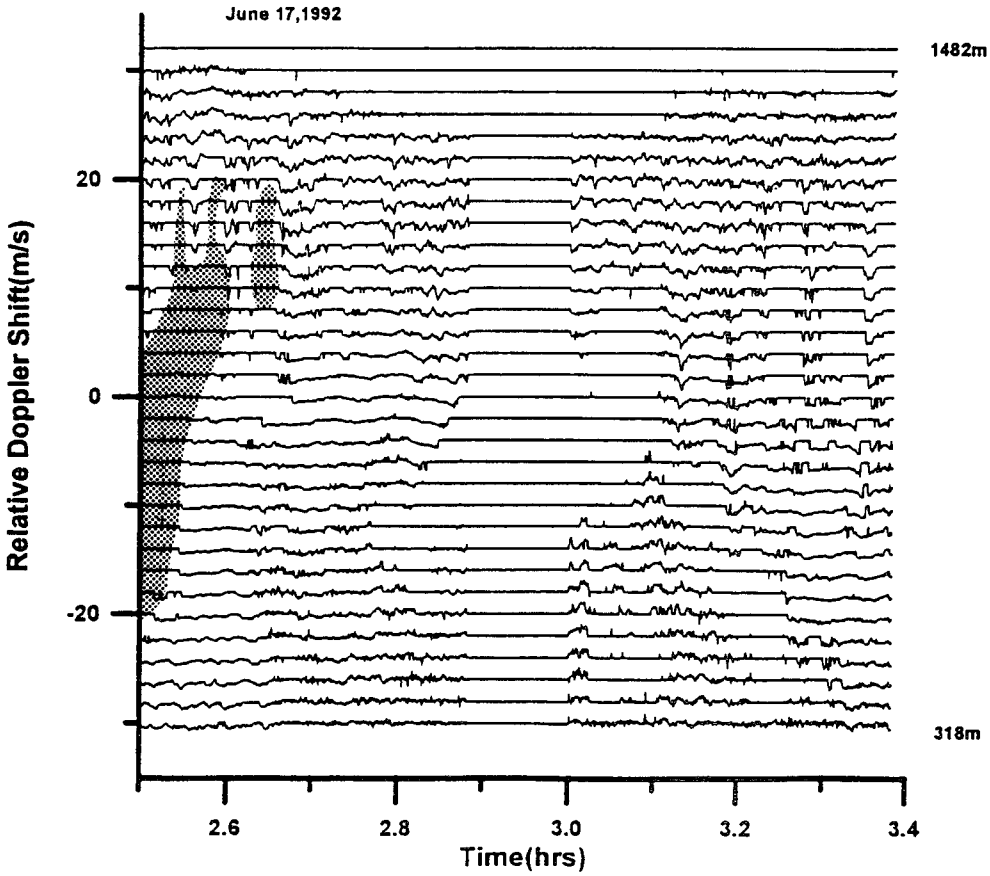

FIG. 4a. Nightime vertical wind speed for range gates 3–34. The measurement at each range gate has been offset by 2 m s^{-1} relative to the adjacent range gate. Straight line unshaded areas are regions of no signal and shaded straight line areas are regions where the reflectivity was above the threshold of −17 dBZ. The space between 2.88 and 3.0 h is due to the radar antenna being run in a nonvertical mode. The range gate spacing was 37.5 m, and each measurement is made every 3 s.

$$\overline{wT_v}(z) = \frac{\overline{(wT_v)_{z_2}}}{\delta z}(z - z_1), \qquad (14)$$

where $\delta_z = z_2 - z_1$, we obtain

$$w_*^3 = 2.5\,\frac{g}{T_v}\,\overline{(wT_v)_{z_2}}\,\frac{\delta z}{2}. \qquad (15)$$

Substituting (12) into (15) and solving for the virtual temperature flux at cloud top,

$$\overline{(wT_v)_{z_2}} \approx 3.16(\sigma_w^3)_{\max}\frac{T_v}{g\,\delta z} \approx 97(\sigma_w^3)_{\max}/\delta z. \qquad (16)$$

For the daytime case (1200–1530 UTC 17 June 1993), δz in (14), (15), and (16) ≈ 230 m and σ_w^2 ≈ 0.11 $m^2\,s^{-2}$. This gives $-(\overline{wT})_{z_2} \approx 0.012$ K m s^{-1}. For the nighttime case (six selected 23-min periods between 0030 and 0430 UTC 17 June 1993), $\delta z \approx 400$ m and $\sigma_w^2 \approx 0.19$ $m^2\,s^{-2}$, which gives $-(\overline{wT})_{z_2}$ ≈ 0.018 K m s^{-1}. We can compare the daytime results with the average of Nicholls's (1989) five cases over the North Sea. He obtained $-(\overline{wT_v})_{z_2} \approx 0.015$ K m s^{-1} with $\delta z \approx 630$ m. The virtual temperature fluxes are in good agreement, considering that shortwave warming in June at the lower latitude of Porto Santo is greater than over the North Sea and, therefore, might account for the somewhat smaller virtual temperature flux. The higher virtual temperature flux for the nighttime case is consistent with the absence of compensating shortwave warming.

In contrast to the results here, Nicholls obtained a variance profile that indicated that the buoyancy generated by radiative cooling extended to below cloud base. Thus, in his clouds, which in general were not as thick as those considered here, mixing extends throughout the depth of the cloud. This is reflected in the larger liquid water contents of the clouds observed by Nicholls (1989). In general, he found nearly adiabatic liquid water contents, ranging from about 0.2 to 0.4 g kg^{-1} near cloud top, whereas in

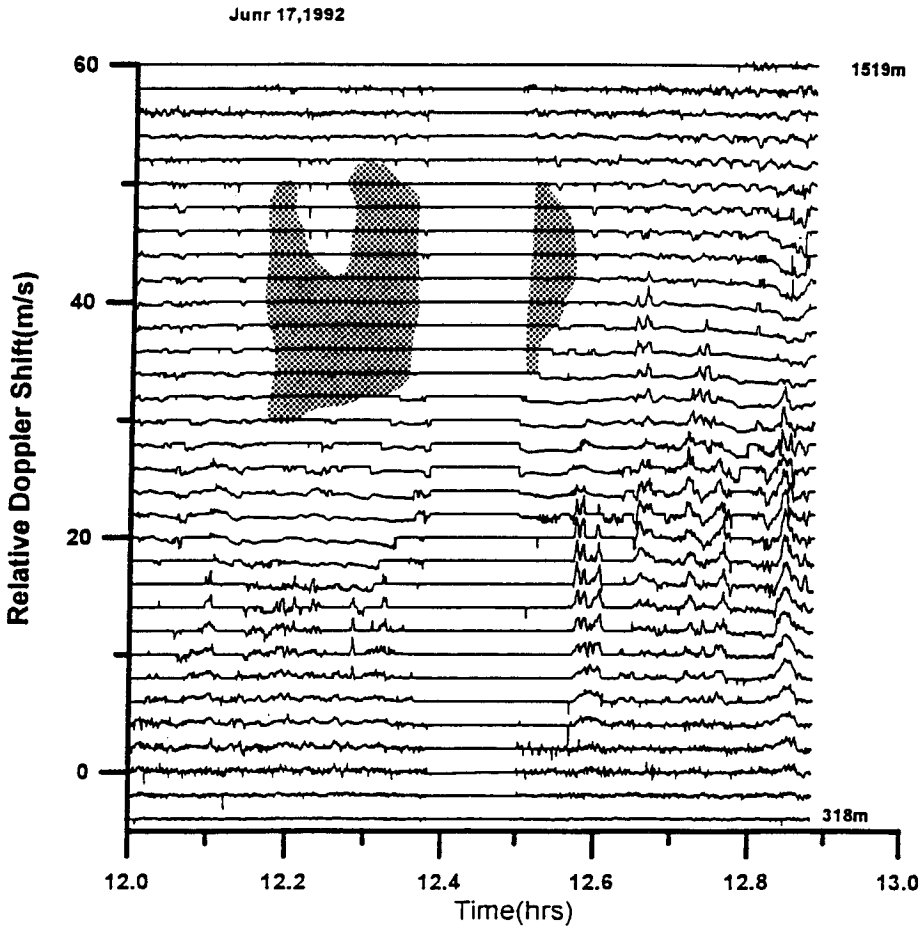

FIG. 4b. Daytime vertical wind speed for range gates 3–35. The measurement at each range gate has been offset by 2 m s^{-1} relative to the adjacent range gate. Straight line unshaded areas are regions of no signal where the reflectivity was above the threshold of −17 dBZ. The space between 12.38 and 12.50 h is due to the radar antenna being run in a nonvertical mode. The range gate spacing is 37.5 m, and each measurement is made every 3 s.

ASTEX we find about 0.1 g kg^{-1} in some of the measurements analyzed so far (Frisch et al. 1995). Nicholls (1989) also found highly variable numbers and average radii of cloud droplets, as expected in a region that might be subject to anthropogenic sources of CCN (cloud condensation nuclii). By comparison the ASTEX cloud cover observed here is optically thinner, farther from adiabatic (which indicates less mixing—especially through the entire cloud), and has relatively fewer droplets, which is characteristic of unpolluted air. It is likely that this is mainly a consequence of our selection process, which excludes clouds with drizzle. Thus, the cases considered here are complementary to the Nicholls and Leighton (1986) cases in that these cases characterize a nondrizzle, pristine, CCN stratiform cloud layer. In our case, radiatively driven cloud-top buoyancy flux is insufficient to generate a thoroughly mixed cloud layer.

6. Discussion

This technique of using a cloud-sensing Doppler radar appears promising for the measurement of the vertical component of turbulence in stratus clouds. We have shown that by using the radar reflectivity as an indicator of larger droplets we can measure turbulent air motions in cloud for reflectivity less than about −17 dBZ. Some of these motions are made up of 100-m-scale updrafts and downdrafts that are vertically coherent for several hundred meters within the cloud. The measurement of w such as displayed in Figs. 4a,b can be extended for many hours. This extension will be useful since it can show the mesoscale variability. This will be a useful complement to LES studies (Moeng et al. 1992).

The average variance and skewness measurements for the day–night cases show some interesting features. First of all, the variance profiles show two maxima in

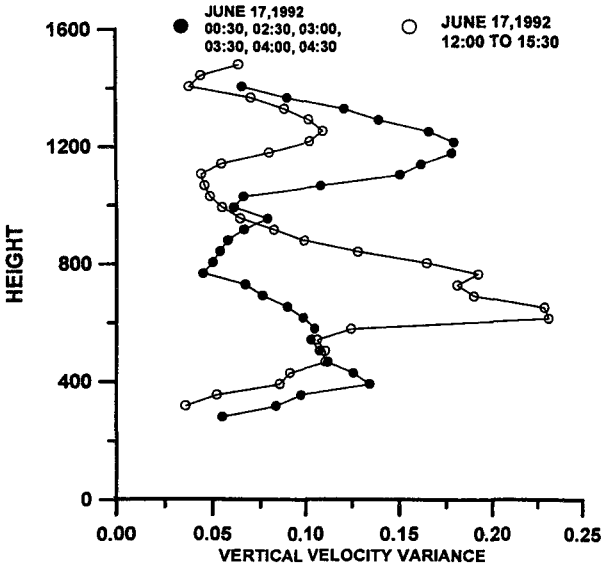

FIG. 5. Vertical velocity variance $m^2 s^{-2}$ vs height for a daytime and nighttime case in stratus cloud.

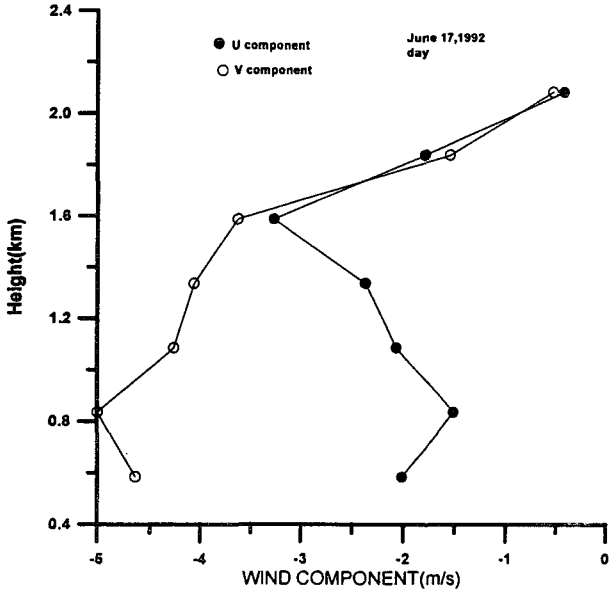

FIG. 7. Wind profiler wind components for the daytime case from near cloud base through cloud top.

both the daytime and nighttime cases. The upper maximum is larger at night than during the day. This day–night difference is consistent with solar shortwave radiation warming the upper part of the cloud, thus diminishing the effect of the longwave cooling at cloudtop and reducing the turbulence generation. The shear of the mean wind is about the same and very small, so it is unlikely that this difference between day and night is due to shear. In addition, the skewness in this part of the cloud is negative, consistent with a cooling cloud top both for the day and night cases. In the lower part of the cloud, the skewness is positive, consistent with a convective layer heated from below. The lower maximum in the vertical velocity variance is greater during the day than at night. These maxima are similar to some of those found by Nicholls (1984), who used aircraft flights at several heights to determine the vertical velocity variance. In his observations there

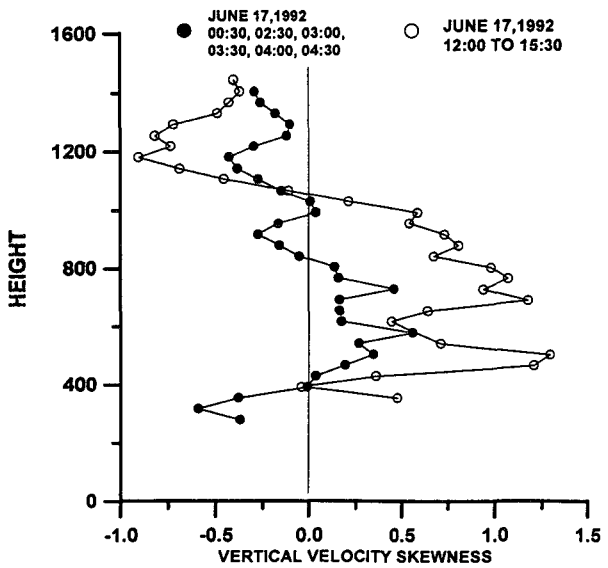

FIG. 6. Vertical velocity skewness vs height for a daytime and nightime case in status cloud.

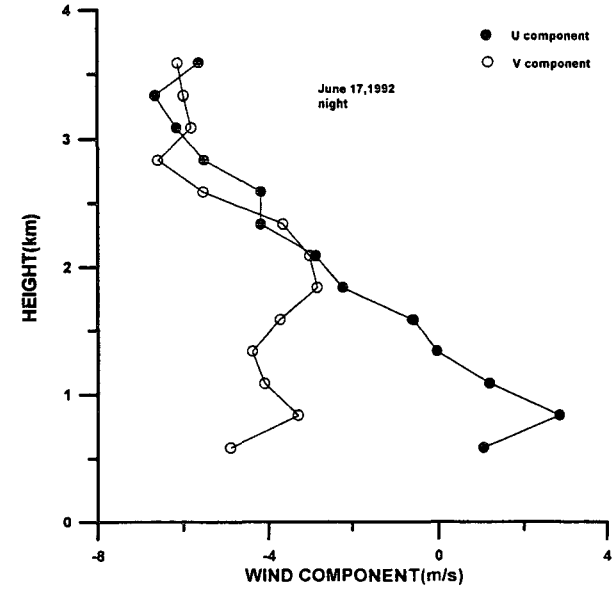

FIG. 8. Wind profiler wind components for the nightime case from near cloud base through cloud top.

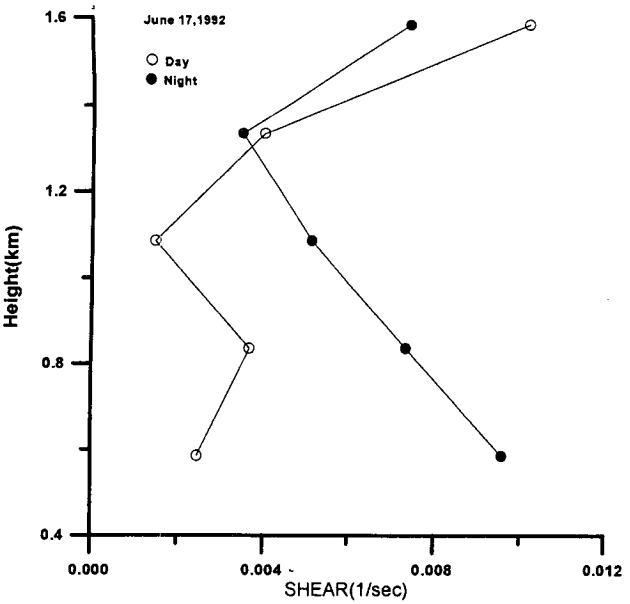

FIG. 9. Wind profiler vertical wind shear for the daytime and nighttime cases.

were two maxima, one near cloud top with a magnitude of about 0.1 $m^2 s^{-2}$ and another below cloud base with a maxima of about 0.2 $m^2 s^{-2}$. A separate stratus study by Hignett (1991), with vertical velocity measurements from a tethered balloon, shows profiles of day–night variances with similar behavior. In his case, the nighttime maximum was about 0.25 $m^2 s^{-2}$, while the daytime maximum was about 0.06 $m^2 s^{-2}$. In the daytime case, there was a suggestion of a lower maximum below cloud base.

Acknowledgments. We wish to thank Bob Kropfli and Steve Cox for their support of this work; Bruce Bartram for the excellent engineering support; Ilga Paluch for helpful comments, discussion, and review of our manuscript; and Chin-Hoh Moeng, Qing Wang, Paul Ciesielski, and Steve Siems for some very helpful discussions. This work was partially funded by the National Oceanic and Atmospheric Administration's Climate and Global Change Program, by the Department of Energy's Atmospheric Radiation Measurement Program, and by ONR N00014-90-F0037 under Interagency Agreement 89-12.

REFERENCES

Atlas, D., D. Short, and D. Rosenfeld, 1989: Climatologically tuned reflectivity–rain rate relations. *Proc. 24th Conference on Radar Meteorology,* Tallahassee, FL, Amer. Meteor. Soc., 666–671.

Battan, L. J., 1973: *Radar Observations of the Atmosphere.* University of Chicago Press, 324 pp.

Borovikov, A. M., 1961: *Cloud Physics.* Gidrometeoizdat, 459 pp.

Brost, R. A., J. C. Wyngaard, and D. H. Lenschow, 1982: Marine stratocumulus layers. Part 2: Turbulence budgets. *J. Atmos. Sci.,* **39,** 818–836.

Caughey, S. J., and M. Kitchen, 1984: Simultaneous measurements of the turbulent and microphysical structure of nocturnal stratocumulus cloud. *Quart. J. Roy. Meteor. Soc.,* **110,** 13–34.

Davidson, K. L., C. W. Fairall, P. Jones Boyle, and G. E. Schacher, 1984: Verification of an atmospheric mixed-layer model for a coastal region. *J. Climate Appl. Meteor.,* **23,** 617–636.

Deardorff, J. W., 1980: Stratocumulus-capped mixed layers derived from a three dimensional model. *Bound.-Layer Meteor.,* **18,** 495–527.

Frisch, A. S., C. W. Fairall, and J. B. Snider, 1995: Measurement of stratus cloud and drizzle parameters in ASTEX with a K_α-band Doppler radar and microwave radiometer. *J. Atmos. Sci.,* **52,** 2788–2799.

Hignett, P., 1991: Observations of diurnal variation in a cloud-capped marine boundary layer. *J. Atmos. Sci.,* **48,** 1474–1482.

Levin, L. M., 1961: *Studies of Physics of Large Aerosols.* USSR Academy of Sciences, 267 pp.

Moeng, C.-H., S. Shen, and D. A. Randall, 1992: Physical processes within the nocturnal stratus-topped boundary layer. *J. Atmos. Sci.,* **49,** 2384–2401.

Nicholls, S., 1984: The dynamics of stratocumulus: Aircraft observations and comparisons with a mixed layer model. *Quart. J. Roy. Meteor. Soc.,* **110,** 783–820.

——, 1988: The structure of radiatively driven convection in stratocumulus. *Quart. J. Roy. Meteor. Soc.,* **115,** 487–511.

——, and J. Leighton, 1986: An observational study of the structure of stratiform cloud sheets: Part I. Structure. *Quart. J. Roy. Meteor. Soc.,* **112,** 431–460.

Slingo, A., R. Brown, and C. L. Wrench, 1982a: A field study of nocturnal stratocumulus: III. High resolution radiative and microphysical observations. *Quart. J. Roy. Meteor. Soc.,* **108,** 145–165.

——, S. Nicholls, and J. Schmetz, 1982b: Aircraft observations of marine stratocumulus during JASIN. *Quart. J. Roy. Meteor. Soc.,* **108,** 833–855.

Wang, Q., and B. A. Albrecht, 1994: Observations of cloud-top entrainment in marine stratocumulus clouds. *J. Atmos. Sci.,* **51,** 1530–1547.

White, A. B., C. W. Fairall, and D. W. Thomson, 1991: Radar observations of humidity variability in and above the marine atmospheric boundary layer. *J. Atmos. Oceanic Technol.,* **8,** 639–658.